Quesnel, Y. et al. (2020), Geophysical Signature of the Tunnunik Impact Structure, Northwest Territories, Canada. *Meteoritics and Planetary Science*, 1-16, doi:10.1111/maps.13447

Geophysical Signature of the Tunnunik Impact Structure, Northwest Territories, Canada

Y. Quesnel[1], W. Zylberman[1,2], P. Rochette[1], M. Uehara[1], J. Gattacceca[1], G. R. Osinski[2,3], Dussouillez, P.[1], Lepaulard, C.[1] and C. Champollion[4]

[1]Aix-Marseille Univ, CNRS, IRD, INRAe, Coll France, CEREGE, Aix-en-Provence, France.

[2]Institute for Earth and Space Exploration, University of Western Ontario, London, Ontario N6A 5B7, Canada

[3]Department of Earth Sciences, University of Western Ontario, London, Ontario N6A 5B7, Canada

[4]Geosciences Montpellier, UMR5243, Université de Montpellier – CNRS, Place E. Bataillon, 34095 Montpellier, France

Corresponding author: Yoann Quesnel (quesnel@cerege.fr)

Key Points:

- A 3 mGal negative gravity anomaly and a 120 nT positive magnetic anomaly were measured over the center of the Tunnunik impact structure
- A numerical model constrained by laboratory measurements on rock samples suggests an uplifted magnetic crystalline basement
- The fracturing/brecciation extends down to 1 km in depth

Abstract

In 2011, the discovery of shatter cones confirmed the 28 km-diameter Tunnunik complex impact structure, Northwest Territories, Canada. This study presents the first results of ground-based electromagnetic, gravimetric and magnetic surveys over this impact structure. Its central area is characterized by a ~10 km wide negative gravity anomaly of about 3 mGal amplitude, roughly corresponding to the area of shatter cones, and associated with a positive magnetic field anomaly of ~120 nT amplitude and 3 km wavelength. The latter correlates well with the location of the deepest uplifted strata, an impact-tilted Proterozoic dolomite layer of the Shaler Supergroup exposed near the center of the structure and intruded by dolerite dykes. Locally, electromagnetic field data unveil a conductive superficial formation which corresponds to an 80-100 m thick sand layer covering the impact structure. Based on measurements of magnetic properties of rock samples, we model the source of the magnetic anomaly as the magnetic sediments of the Shaler Supergroup combined with a core of uplifted crystalline basement with enhanced magnetization. More classically, the low gravity signature is attributed to a reduction in density measured on the brecciated target rocks and to the isolated sand formations. However, the present-day fractured zone does not extend deeper than ~1 km in our model, indicating a possible 1.5 km of erosion since the time of impact, about 430 Ma ago.

Plain Language Summary

This study reveals the geophysical signature of the buried structure of an eroded impact crater, Tunnunik, located in Northwest Territories, Canada. A positive magnetic anomaly was detected at the center, showing the uplift of some deep geological formations and the possible presence of strongly-magnetized basement. A negative gravimetric anomaly is also observed, mostly corresponding to the fracturing/brecciation of the impacted rocks inside the crater. Using numerical models constrained by laboratory measurements on rock samples, the physical properties and geometry of the buried geological formations are estimated. An important implication of this study is the link between the geophysical remains of an impact crater and the post-impact erosion.

INTRODUCTION

With about 190 impact structures confirmed, the Earth presents currently the lowest number of craters of all the terrestrial planets. Indeed, craters on Earth are continuously removed by erosion and hidden by sedimentation, and/or tectonic activity (Grieve 2006; Hergarten and Kenkmann 2015). Therefore, geophysical methods are particularly relevant to the study of terrestrial impact craters, as they can reveal buried or eroded structures (Pilkington and Grieve 1992; Gudlaugsson 1993; Grieve and Pilkington 1996; Pilkington and Hildebrand 2000; Kjaer et al. 2018). They also help to unveil the physical effects of syn- and post-impact processes which are still not completely understood, particularly for mid-size to large impact structures (Osinski and Pierazzo 2013). Moreover, they help to reveal the present-day geometry of the different layers of impact lithologies.

The most commonly used geophysical techniques for studying impact craters are gravity and magnetic surveys by satellites, airplanes and/or ground measurements. Indeed potential-field anomalies are often significant over impact structures, even buried or eroded. Small-size (apparent diameter $D_a < 10$ km; D_a being the present-day diameter after erosion of the final crater rim) impact craters are well characterized by negative potential field anomalies (Grieve and Pilkington 1996), while it is not as clear for intermediate-size ($10 < D_a < 30$ km) complex impact structures. The low gravity signature is due to a reduction in the density of target rocks because of impact-induced fracturing, brecciation and melting due to the compression, excavation and modification stages of the impact event (Pilkington and Grieve 1992; Osinski and Pierazzo 2013). Additional minor effects can also contribute to the mass deficiency, such as lower-density post-impact sedimentary layers filling relatively fresh craters (Grieve and Pilkington 1996). The lithological and physical changes associated with the impact process can also be modified by post-impact alteration. The observed weak magnetic signature over small craters ($D_a < 10$ km) results from the alteration of the pre-existing regional signals (Cisowski and Fuller 1978; Clark 1983; O'Neill and Heine 2005), but may be also influenced by the reduction of the natural remanent magnetization (NRM) through partial or complete shock remagnetization (Gattacceca et al. 2010). Overall, some of the impact induced effects on rock magnetism are still debated, such as the possible preservation of a shock-induced remanent magnetization (SRM; e.g., Cisowski and Fuller 1978; Halls 1979; Pesonen et al. 1992; Gattacceca et al. 2007, 2008, 2010; Tikoo et al. 2015). For larger craters ($D_a > 10$ km), central high-amplitude and short-wavelength anomalies are observed (Pilkington and Grieve 1992; Morgan and Rebolledo-Vieyra 2013). Their source is usually complex, and can originate from shock metamorphism (e.g., Slate Islands and Charlevoix, see Halls 1979; Robertson and Roy 1979; review in Grieve and Pilkington 1996), cooling of impact-melt rocks and/or breccias (e.g., Ries and Morokweng; Pohl et al. 2010; Henkel et al. 2002), structural deformation of target geological units during the modification stage (e.g. Bosumtwi; Ugalde et al. 2007), and/or post-impact hydrothermal processes (e.g., Haughton: Quesnel et al. 2013; Zylberman et al. 2017; Clearwater Lakes: Gattacceca et al. 2019). Henkel (1992) and Henkel and Reimold (2002) also suggested oxidation of pre-existing magnetic carrier phase in the strongly fractured rocks, which may explain the reduction of ground magnetic susceptibilities surrounding the central uplift. The origin of magnetic anomalies with a significant negative part in complex and eroded impact structures remains unclear (Pilkington and Grieve 1992; Grieve 2006). All larger craters ($D_a > 40$ km) show high-amplitude magnetic anomalies at their center (Pilkington and Grieve 1992; Morgan and Rebolledo-Vieyra 2013).

It is notable that the magnetic and gravimetric anomaly characterization strongly depends on the altitude of the measurements: no signature at satellite or airborne altitude does not mean that there are no contrasts in the upper crust of the studied area. For instance, this effect has been suggested to explain the lack of 'apparent' magnetic signatures of Hellas and Argyre large impact basins on Mars (Acuña et al. 1998), even if the absence of a dynamo during the cooling stage after these events is a better explanation (Langlais et al. 2004; Langlais and Thébault 2011). This may also be suggested for most of the magnetic signatures of lunar impact structures: the lowest satellite magnetic field measurements were performed at minimum 30 km of altitude, excluding *de facto* the mapping of small-wavelength magnetized contrasts (Nicholas et al. 2007; Hemingway and Tikoo 2018), while a wealth of gravimetric details were observed by the GRAIL mission (Zuber et al. 2016). On Earth, few large impact structures – including Chicxulub (Gulick et al. 2013) - exhibit a gravimetric anomaly that can be observed by satellite measurements. For

mid-size impact structures, the characterization of gravimetric and magnetic anomalies by airplane/helicopter measurements can be possible to get a broad overview of its geophysical signature. However, such airborne surveys are still low-resolution, practically difficult and expensive for studying remote areas. Ground surveys allow acquiring high-resolution gravimetric and magnetic data over impact structures in remote areas. also enable sampling to be conducted for further laboratory analyses, to update the geological mapping and to identify possible local geophysical anomalies (e.g., the Haughton crater center; Zylberman et al. 2017). All these data will serve as constraints for modeling the geological (and possibly multiple) sources of the observed gravimetric and magnetic anomalies. The central uplift itself creates a gravimetric anomaly, but on Earth, the erosion level of the impact structure will then play a role. In most cases, the more eroded the crater, the less significant (in wavelength and amplitude) the gravimetric negative anomaly (Pilkington and Grieve 1992). On the other hand, the erosion of a large thickness of post-impact sediments will better unveil density and magnetization contrasts linked to pre-, syn- or post-impact processes in the structure.

In this study the first ground geophysical measurements acquired over the recently-discovered mid-size (D_a ~ 28 km) eroded Tunnunik impact structure are described, analysed and modeled in terms of geological structure and cratering processes.

GEOLOGICAL CONTEXT

The Tunnunik impact structure is located in the western Canadian Arctic Archipelago (Fig. 1) just south of the Richard Collinson Inlet ("Tunnunik" in Inuvialuit), on the Prince Albert peninsula, northwestern Victoria Island (75°28'N, 113°58'W). The target sequence is composed of sub-horizontal Cambro-Silurian sedimentary rocks (mostly carbonates) from the Arctic Platform: from oldest to youngest, the Wynniatt (part of the Shaler Supergroup), Mount Phayre, Victoria Island, and Allen Bay formations (Fig. 1; Dewing et al. 2013; Newman and Osinski 2016). Neoproterozoic diabase dykes also intrude into the Wynniatt Fm. More detailed information on the pre-impact stratigraphic sequence and geological context can be found in Dewing et al. (2013). There are also a number of Quaternary sand and gravel formations (not shown in Fig. 1) deposited between 50 and 100 m in altitude throughout the crater interior, and mainly related to the central river valley where some outcrops of the Shaler Supergroup and Mount Phayre formations show a central uplift. By using remote sensing and sample analyses, this formation was recently mapped as fluvioglacial deposits (Unit 1 of Choe et al. 2019). Sea shells were found in some outcrops of this formation, suggesting that it could correspond to post-glacial marine deltaic deposits, now overwater due to the isostatic rebound. Based on the observation of tilted strata and the distribution of shatter cones, Dewing et al. (2013) described a ~25 km-wide circular feature. Based on detailed mapping and the presence of inward-dipping listric faults out to a radius of 14 km, Osinski et al. (2013) defined a 28 ± 0.5 km apparent crater diameter (D_a). No crater fill breccias and/or melt rocks were mapped, indicating that the impact structure is deeply eroded. Only isolated dykes of polymict impact breccias were observed (Newman and Osinski 2016). Paleomagnetic analyses of these dykes has providedan age for the impact event of 440±10 Ma (Lepaulard et al. 2019). The present topography decreases from about 200 m altitude in the southeast corner to the sea level of the Richard Collinson Inlet in the northwest. This general trend is cut by two major ~N-S oriented rivers - including one in the

central part of the structure – and by syn-impact (mainly concentric) and post-impact (mainly in the SW-NE direction) faults. Therefore, except for the concentric faults, there is no topographical and geomorphological signature of an impact crater. Possible hydrothermal alteration has also been reported within the impact structure, but evidence remains sparse and samples are still under investigation, as it is not always clear if the described alteration is pre- or post-impact (Marion et al. 2013).

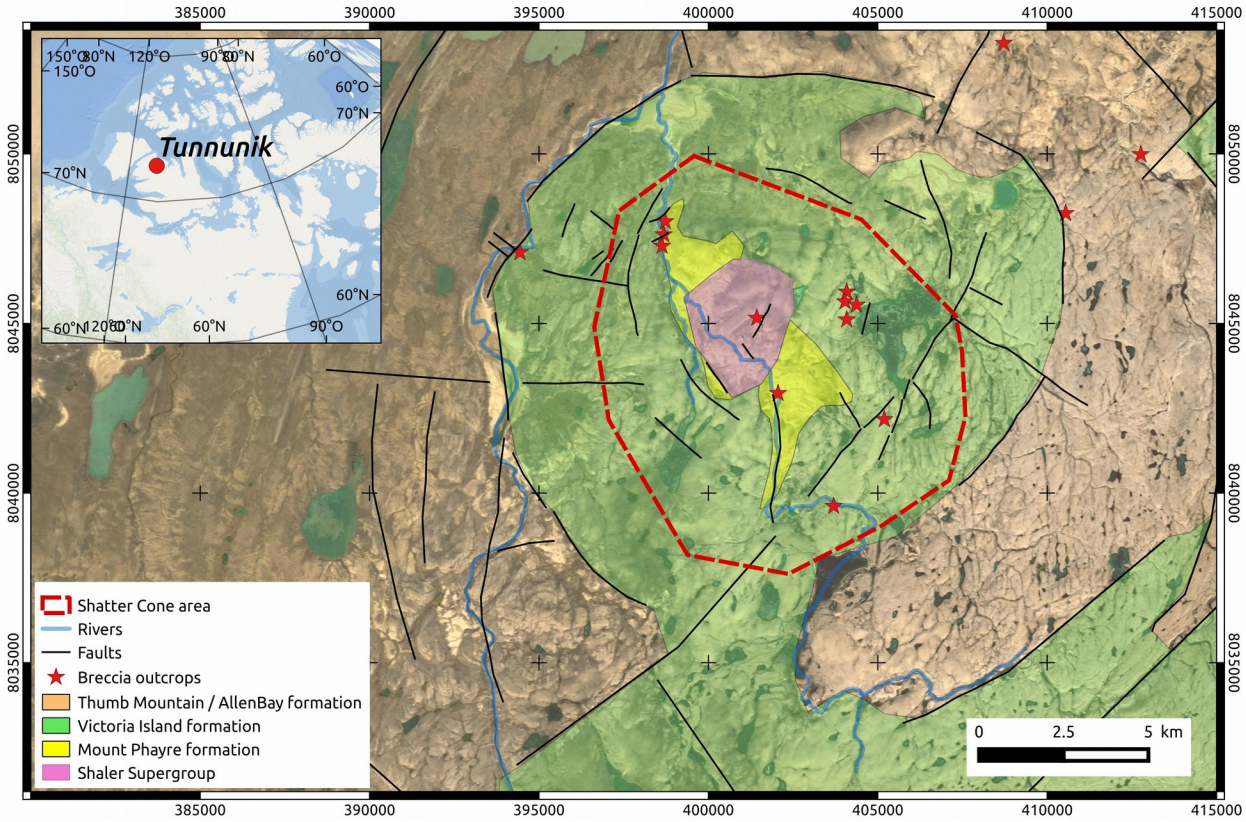


Fig. 1. Geological map of the Tunnunik impact structure, modified from Dewing et al. (2013) and Newman and Osinski (2016). Background corresponds to a Map Data ©2015 Google satellite image. Stratigraphy: Shaler Supergroup (Neoproterozoic), Mount Phayre formation (Cambrian), Victoria Island formation (Cambrian/Ordovician), and Thumb Mountain/Allen Bay formation (Upper Ordovician/Silurian). The coordinate system for the geological map is UTM Zone 12 North projection with WGS84 datum, in meters. Upper left: Location of the structure on Victoria Island in the Canadian Arctic, with a geographic coordinate system on a WGS84 datum. Background corresponds to the ArcGIS online ESRI Ocean layer.

METHODS

Ground gravity and magnetic field measurements (total paths of 300 km) were performed within the central part of the Tunnunik impact structure, in an area approximately corresponding to the extent of the Victoria Island Formation (Fig. 2). The wide N-S river on the western side prevented further measurements in that direction, while the large area and a short time in the field in this remote Arctic region also influenced our choice to mainly survey the center of the

structure. Thus we obtained a well constrained map of the central part rather than extended profiles. We also conducted local subsurface electromagnetic sounding in order to determine the thickness of quaternary surficial formations that could influence the gravity signature.

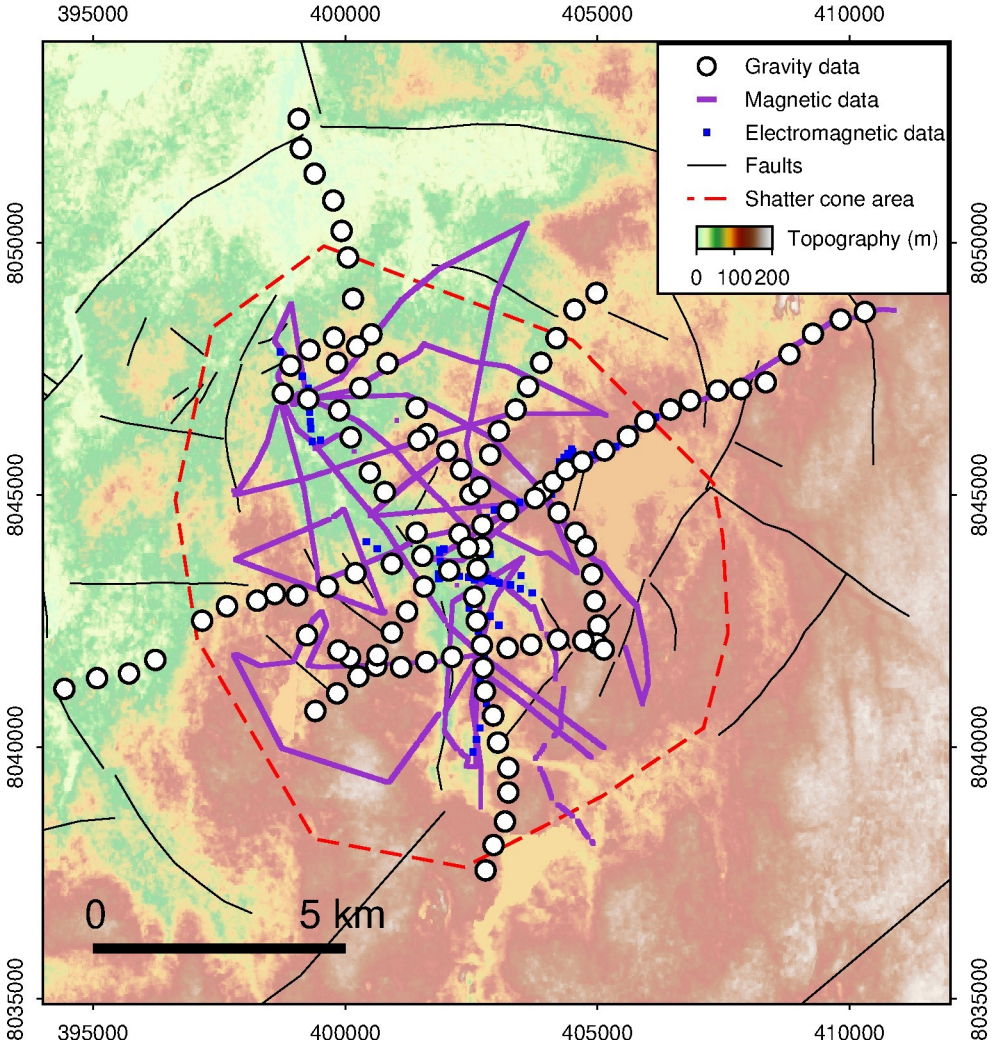


Fig. 2. Geophysical measurements performed at Tunnunik. Background corresponds to a digital elevation model version 2 (GDEM2) from ASTER (NASA-METI). Same coordinate system as for Fig. 1.

The gravity field was measured using a Scintrex CG-5 Autograv gravity meter. Three main profiles in the NNW-SSE, NE-SW and WSW-ENE directions were performed with a mean spacing of 500 m between each measurement point. These profiles cross each other near the estimated center of the structure. Additional measurements along 5 shorter profiles, with

acquisition spacing between 250 and 500 m, completed the central part of the gravity map. A total of 113 independent measurements were acquired. For each point, the gravity field was measured 4 times during 100 seconds at 1 Hz, excluding outliers and outputting the mean value. Instrumental error (i.e. 1 sigma uncertainty), as defined by the standard deviation of the 4 successive averages, varied between 0.5 and 16 µGal with a mean value of 6 µGal, depending on wind and soil stability. Depending on the number of acquired measurements, on the local topography of the surveyed area, as well as on the weather conditions, drift varied from 0.5 to 2.6 µGal mn^{-1} (average: 1.2 µGal mn^{-1}). For each station, the X, Y and Z locations were precisely measured using a differential GNSS Trimble R8 system. The base and mobile GNSS stations were connected by a standard radio communication and monitored with a controller. Due to the long distances and topography, a secondary radio relay station was used to extend the communication with the base station. With the real-time kinematics (RTK) capability of the system, a precision of ±10 cm in elevation (Z) was achieved. This precision is suitable for gravity accuracy at the 0.1 mGal level as an elevation error of 10 cm produces a 0.03 mGal error in free-air gravity (Featherstone and Dentith 1997). Then the Bouguer correction (0.1 mGal/m, opposite sense to free-air) will reduce this error to 20 µGal, which, combined with the average 6 µGal experimental error of the CG-5 instrument, would result in a total error inferior to 30 µGal. This total error is below 1% of the total amplitude of our Bouguer gravity anomaly (see next sections). Gravity data were processed using the dGNSS elevation data and a series of standard corrections to remove the Earth tide, drift, latitude, altitude and topographic effects and finally, to obtain the complete Bouguer gravity anomaly value. The final accuracy of the Bouguer anomaly (taking into account instrumental errors, altitude and topography correction accuracies) is 0.1 mGal (see the Supplementary Material for details about gravity data processing, and Figs. S1 and S2; GEOINT 2008; Heiskanen and Moritz 1967; Hwang et al. 2003; Schwiderski 1980; Tamura 1987; Wenzel 1996).

The variations of the intensity of the geomagnetic field vector (Total Magnetic Intensity, TMI) were mapped using a mobile Geometrics G-858 MagMapper cesium vapor probe fixed at 2 m height on a pole. The internal and external field temporal variations on site were measured using a fixed Geometrics G-856 proton precession base station magnetometer. The use of a base station for diurnal variation of the magnetic field was necessary due to the proximity of the North magnetic pole (1,700 km away): diurnal variations reached several hundreds of nT of amplitude during our surveys, potentially completely concealing the crustal signal, which is in the range of 0 to 100 nT in amplitude. The G-856 and G-858 magnetometers have absolute precision of 0.1 and 0.01 nT (at 1 Hz sampling rate), respectively. A mean sampling rate of 15 s was used on the field leading to a mean spatial resolution of ~20 m along each survey line. The surveyed area was mainly restricted to the central part within the shatter cone area, except for one ENE-WSW line which extends towards the northeast faults (Fig. 2). During the survey the IGRF predicted average field was about 58140 nT in intensity - exactly in the range of our base station data - 86° and 16° of inclination and declination, respectively. Given the magnetic north pole was 1,700 km away, there was no need to apply the reduction-to-the-pole to our magnetic field data. The magnetic field anomaly was then simply computed by subtracting the TMI value measured at the base station from the TMI value acquired by the mobile magnetometer. We carefully checked that there was no correlation of the anomaly spatial variations with the topography. The poor spatial resolution of the available airborne data (CAN-SCAN project 1965-1976) and magnetic field grids in this area (Ravat et al. 2009) prevents from a good characterization and comparison of the regional influence over the impact structure. Therefore, we first applied a low-pass (100

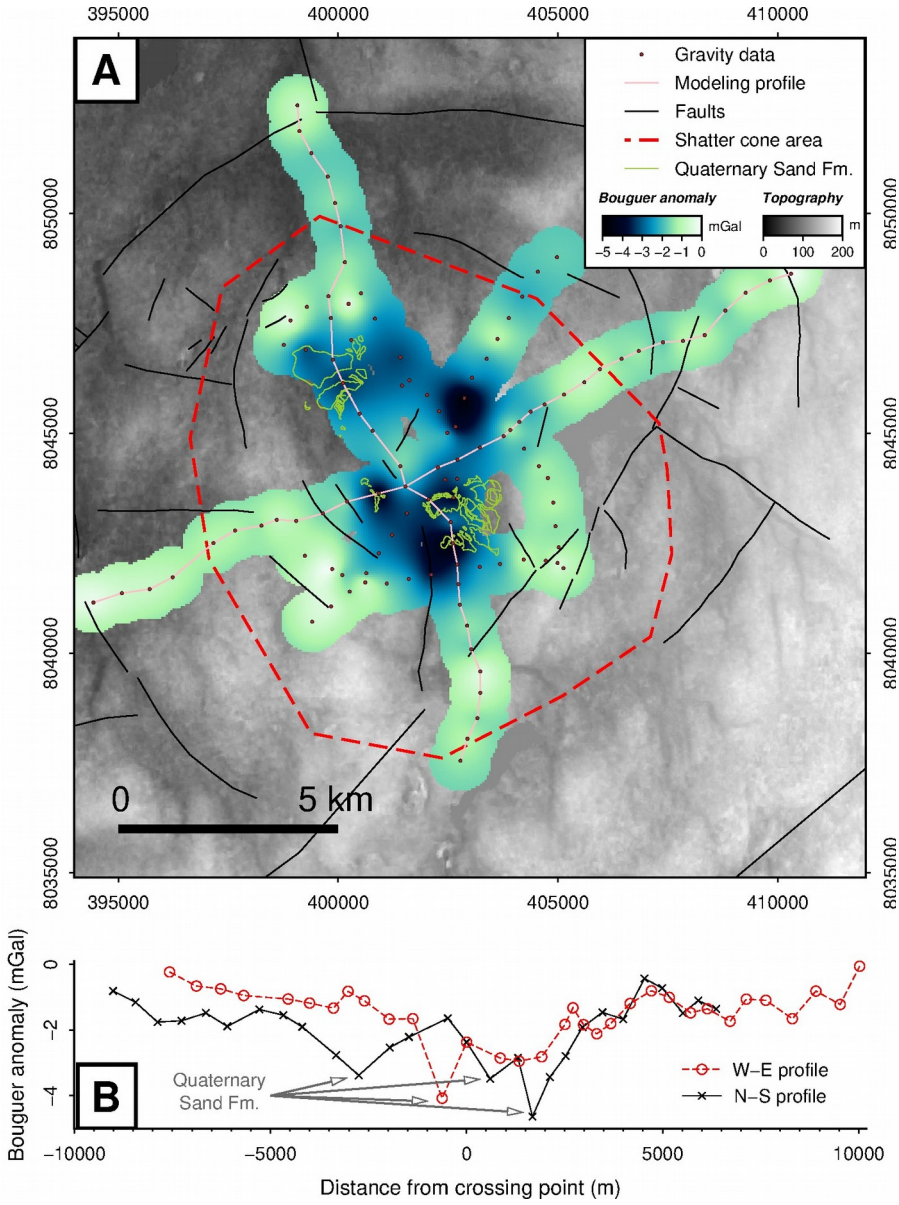
m) filter to the interpolated data grid to exclude isolated outliers, and then detrended this grid by a 3rd-order polynomial surface to level the anomaly map (i.e. to remove an eventual large-scale regional crustal field signal).

Local electromagnetic soundings were performed using the Geonics Ltd EM34-3 terrain conductivity meter, which measures the apparent conductivity (sensitivity of 1000 $mS.m^{-1}$) of the ground by means of a pair of coils. We measured 104 data points to characterize the lateral and vertical extent of quaternary sand deposits at different locations nearby the main central river (Fig. 2). Both horizontal and vertical dipole configurations were implemented at distances of 10, 20, and 40 m between the transmitter and receiver coils, to increase the investigated depth (see Supplementary Material; McNeill 1980). The mean distance between each measurement point was 250 m.

In addition to these geophysical data, we also sampled all accessible lithologies to measure some petrophysical properties in laboratory in order to constrain numerical models of the geological sources of the observed geophysical anomalies. The bulk density of these samples was measured using a Quantachrome Helium stereopycnometer. Magnetic parameters used to constrain the model are described in Lepaulard et al. (2019): the remanent magnetization intensity was obtained from measurements with a Superconducting Quantum Interference Devices (SQUID) 760R (2G Entreprises) magnetometer while the magnetic susceptibility was measured with an AGICO Kappabridge MFK1.

RESULTS AND INTERPRETATION

The complete Bouguer gravity anomaly map is shown in Fig. 3A. It was generated using a minimum curvature interpolation and masking areas with no data. Despite the influence of radial line surveys, the map reveals a general negative gravity anomaly of ~3 mGal amplitude and ~10 km of wavelength over the center of the Tunnunik impact structure. In the absence of data outside of the surveyed area, we cannot infer that this is the maximum amplitude of the anomaly observed over this impact structure (i.e. 3 mGal is a lower limit for the amplitude of the anomaly). In detail, the shape of this central anomaly does not appear to be circular but seems slightly more extended in the N-S direction. The minimum value of -4.6 mGal is also not at the center but is located in a ring of about -4 to -4.5 mGal anomalies surrounding a less negative (–2.5 mGal) isolated central anomaly; this is considered to be located near the center of the structure (402000, 8044000). Fig. 3A shows that most of the concentric negative extrema correspond to the Quaternary sand deposits, suggesting that this porous formation may locally amplify the general low gravity signal at the center. Fig. 3B shows that 5 km away from the center, the anomaly gradients are less important, but still a small increase is observed at the borders, arguing in favor of a more extended anomaly. Therefore, we conclude that a central negative anomaly is visible, with a possible asymmetric shape and with a possible extension beyond our survey area. This gravity anomaly is not observed in the regional gravity data acquired by the National Research Council of Canada (see Supp. Mat. for details of calculations and regional trends in Fig. S1).



293

294

295 Fig. 3. (A) Complete Bouguer gravity anomaly map over the center of the Tunnunik impact structure. The
296 thin pink lines correspond to the gravity anomaly profiles selected for modeling and shown in (B). Faults
297 are indicated by full black lines. The area where shatter cones were observed and collected is delimited by
298 the dashed red line (Osinski and Ferrière 2016), while the limits of the Quaternary Sand Formation
299 correspond to the thin green lines. Grayscaled background corresponds to the digital elevation model
300 shown in Fig. 2. Same coordinate system as for Fig. 1. (B) Complete Bouguer gravity anomaly data along
301 the selected profiles in (A).

The interpolated map of the total-field magnetic anomaly over the center of the Tunnunik impact structure is shown in Fig. 4A. The data distribution limits the analysis to the central part (i.e. within the shatter cone area) only. The total amplitude of the interpolated and filtered signal reaches 120 nT, with minimum and maximum values of -20 and 96 nT, respectively. The positive part of the anomaly is restricted to the central area of the structure and centered at 401000, 8045000. It correlates well with the Shaler Supergroup (with intruding diabase dykes) outcrops (Fig. 4A). Compared to the gravity anomaly, the center of the positiveanomaly is located ~500 m away in the NW direction, but on average, the observed central negative gravimetric and positive magnetic anomalies overlap. Although less extended than the Bouguer gravity anomaly, the central positive magnetic field anomaly also seems to be slightly asymmetrical with a major axis in the NNW–SSE direction and a minor axis in the WSW–ENE direction, with wavelengths of ~6 and ~4 km respectively. Fig. 4B shows the shape of the anomaly in the N-S and W-E directions, unveiling this weak asymetry.

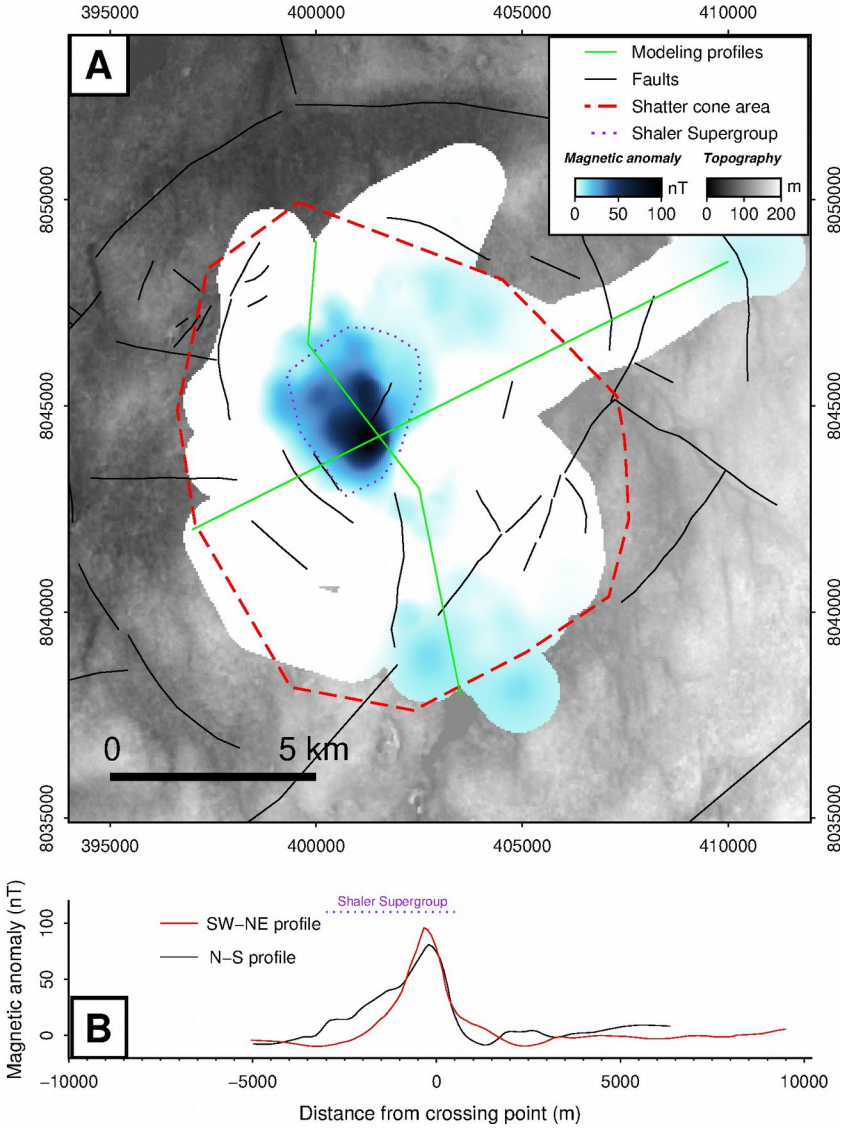


Fig. 4. (A) Magnetic field anomaly map of the center of the Tunnunik impact structure. The green solid line corresponds to the locations of the data selected for modeling. Faults are indicated by full black lines. The area where shatter cones were observed and collected is delimited by the dashed red line (Osinski and Ferrière 2016). The area where the Shaler Supergroup Formation is exposed is delimited by the dotted purple line. Grayscaled background corresponds to the digital elevation model shown in Fig. 2. Same coordinate system as for Fig. 1. (B) Magnetic field anomaly along the selected profiles in (A).

Thus, both gravity and magnetic field signals show a significant anomaly of several km wavelength in the surveyed area. Their correlation argues in favor of a possible single geological source at or nearby the center of the impact structure.

Fig. 5A shows the spatial variations of the subsurface electrical conductivity derived from the electromagnetic measurements performed in the central area of the impact structure (see Supp. Mat. for results of EM surveys performed outside this central part). It clearly reveals that the hills around the center and nearby the river contain porous liquid water loaded material (> 20 mS/m) that contrasts with the resistive frozen soil outside these areas (< 5 mS/m; see Todd et al. 1991 for a comparison in the same environment). The conductive material corresponds to the sand formations either originated from fluvioglacial processes (Choe et al. 2019) or deposited by sea level variations during Quaternary era (Fig. 5B). Within these deposits, variations of the conductivity between 10 and 30 mS/m are observed, reflecting possible variations in the amount of pore water and its salinity eventually due to presence of fossil sea water. Presence of permafrost below the liquid water layer is also a possibility, while permafrost formation above it may have been prevented by a thick dry sand layer (Fig. 5C). The conductivity remains high at the maximum possible depths reached by our measurements, indicating that this sand formation is thicker than 60-80 m. This observation is important because such a thick, weakly dense (2,000 kg m^{-3}), material will decrease the Bouguer gravity value for data acquired on top of (or nearby) this formation. In fact, most of the lowest gravity anomalies correspond to the location of these deposits (see Fig. 5A for an example of the correlation with gravity low values). Still, on kilometric scale, there is a general, centered and negative ~3 mGal Bouguer gravity anomaly over the center of the impact structure.

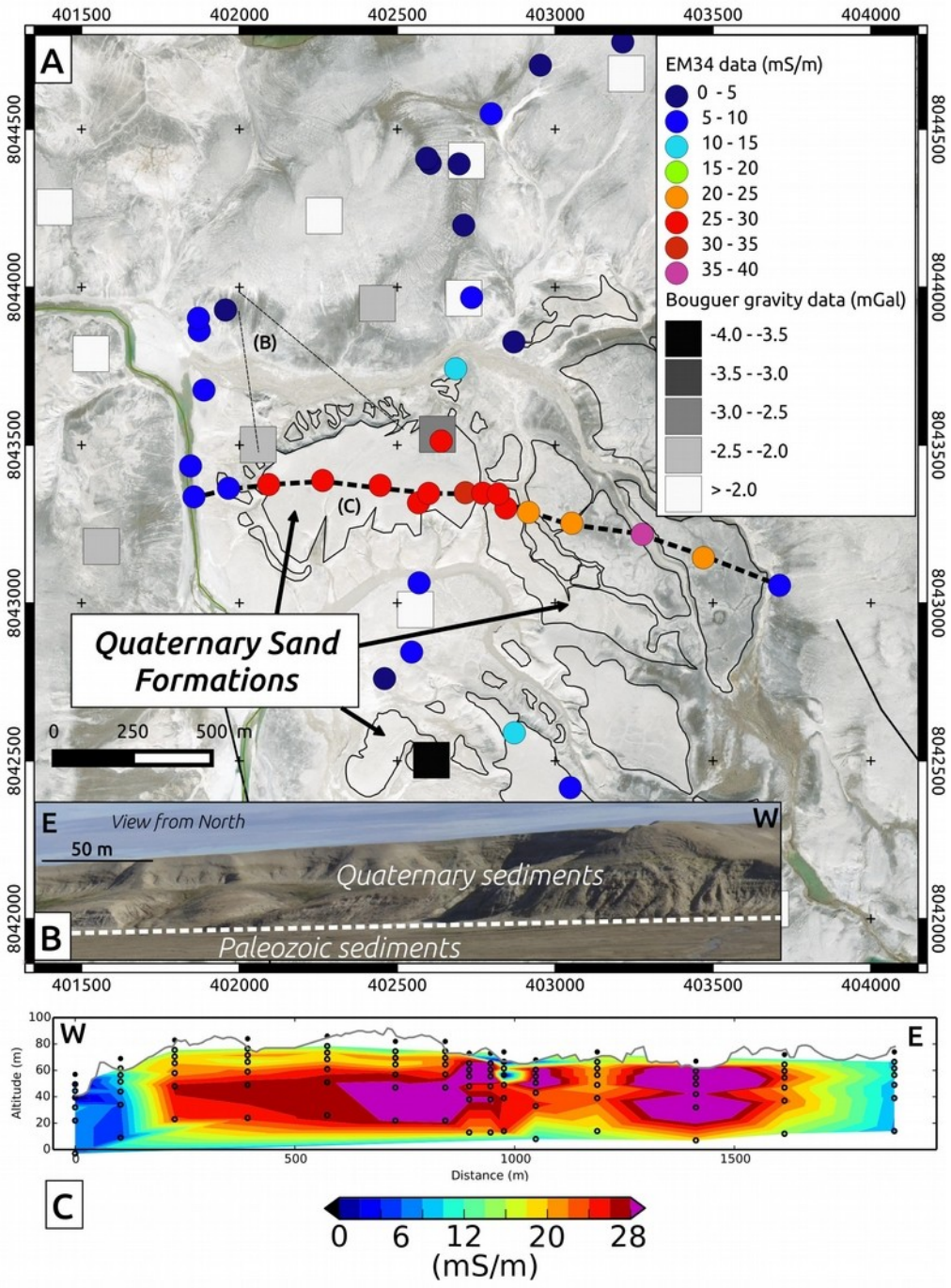


Fig. 5. (A) Map of the electrical conductivity variations at about 20 m in depth, in the central area of the impact structure. Bouguer gravity data are also shown to illustrate the correlation between some isolated low gravity values and the Quaternary Sand deposits. Dashed black line corresponds to the cross-section shown in (C). (B) Image of the conductive formation composed of Quaternary sediments nearby the central river. (C) W-E cross-section resulting from interpolation of conductivity data (vertical exaggeration ~ 2; points: data from different coil orientations at each location) acquired on the sand formation in the same area, along the dashed line in (A).

DISCUSSION

Diameter and erosion

Tunnunik is a mid-size impact structure with a ~10 km wavelength negative Bouguer gravity anomaly of ~3 mGal amplitude over its center. Mid-size complex impact craters (see Osinski and Grieve 2013 for a review) are typically characterized by circular negative gravity anomalies that extend to or beyond the crater diameter. The size and amplitude of the anomaly are expected to increase with an increasing apparent crater diameter D_a (Pilkington and Grieve 1992; Grieve and Pilkington 1996). Since our measurements are limited to the center of the impact structure, they do not reach the outermost faults (outside the map in Fig. 2), which represent the outer limit of D_a, as defined in Osinski et al. (2013). Thus, we can expect a larger amplitude and wavelength of the low gravity signal observed at Tunnunik: the Bouguer gravity data towards the rims still show – in all directions – a small increase before reaching the regional signal (here leveled to 0 mGal). The minimum amplitude of the anomaly (~3 mGal) could reflect a deeply-eroded structure, because impact structures of comparable size generally have a higher amplitude (e.g., 10 mGal for Keurusselkä; Raiskila et al. 2013). Alternatively, this amplitude could be due to the type of target rocks: impact structures in sedimentary targets generally have lower maximum negative Bouguer gravity anomalies (Δg) than those in crystalline targets (Pilkington and Grieve 1992).

Impact structures can be classified using the erosional level index (E) established by Dence (1972; see also Grieve and Robertson 1979) and based on the preservation of their ejecta, crater-fill products and exposure of crater floor (Pilkington and Grieve 1992). Most of the indicated diameters in impact studies are apparent crater diameters D_a (Osinski and Pierazzo 2013). Indeed, the majority of complex impact craters on Earth are eroded (i.e., they are impact structures) and therefore only D_a can be determined in most cases. Tunnunik seems to correspond to the worst state of preservation: indeed the crater floor has been removed and the substructure exposed, with no remnant of ejecta or crater-fill deposits preserved (Dewing et al. 2013; Osinski et al. 2013; Newman and Osinski 2016). The only preserved impact breccia found in the field are in the form of very local and thin (< 1 m of width) dykes injected into the sedimentary target rocks (Osinski et al. 2013; Newman and Osinski 2016). Slightly modifiying the index definition, Osinski and Ferrière (2016) classified the Tunnunik structure as erosion state 6, because of these still visible isolated breccia dikes. Such a deep level of erosion can be either due to a particularly old impact structure or to an especially high rate of erosion, or both. In the present-day periglacial environment of the Canadian High Arctic archipelago (e.g., Lee and Osinski 2005), the 23 Ma Haughton impact structure, located about 900 km away, has been relatively well preserved. Haughton is characterized by a $D_a \approx 23$ km and a smaller estimated rim-to-rim diameter (D) of 16 km (Osinski et al. 2005). Its negative Bouguer gravity anomaly has a 12 mGal amplitude and a 24 km wavelength, the latter being very similar to its D_a (Pohl et al., 1988). It has an erosional level of 2, which means that it is relatively fresh with ejecta partly preserved (Osinski and Ferrière 2016). As mentioned earlier, the diameter of the gravity anomaly should be roughly equal to D_a in relatively fresh craters such as Haughton, while the amplitude - more affected by erosion - is not a relevant criterion (Pilkington and Grieve 1992). Therefore, our gravimetric data suggest that the Tunnunik impact structure is severely eroded, in agreement

with its old age. Indeed, using paleomagnetism, Lepaulard et al. (2019) estimated that this impact event occurred 430-450 Ma ago.

A similarly eroded impact structure is Gosses Bluff in Australia (Barlow 1979), which also formed in sedimentary target rocks. Its apparent crater diameter D_a has been recently revised to 32 km (Osinski and Ferrière 2016). Its total gravimetric anomaly is Δg =–5.5 mGal with a central peak (CP) of –3.5 mGal (Δg = –3 to -4 mGal and CP = –2.5 mGal at Tunnunik). This 142.5 Ma impact structure has been attributed an erosion level similar to Tunnunik (E = 6–7; Pilkington and Grieve 1992; Osinski and Ferrière 2016), while the presence of crater-fill breccias should revise this value to E = 5 (Milton and Sutter 1987). Nevertheless, it shows that the relatively weak amplitude of the remaining gravity anomaly at Tunnunik is not a unique case.

Besides, another phenomenon could explain this feature, without requiring a high amount of erosion. Indeed, diagenetic pressure-solution (Sprunt 1977) could cement the impact-induced fracturation in target rocks buried below a few kilometers of post-impact sediments. To our knowledge, this post-impact phenomenon was never invoked before as a possible way to reduce the amplitude of gravity anomalies in impact structures in sedimentary carbonated rocks. Long term healing of impact induced carbonate porosity by pressure-solution is a well-known phenomena (Croizet et al. 2013) that may be particularly effective in the Tunnunik limestones due to the several hundreds Myr of burial endured by the fractured rock. Moreover, as the impact occurred around 430-450 Ma ago, soon after deposition of the Ordovician sediments, this target may have been not fully lithified, resulting in a lesser amount of fracturing and/or easier healing of fractures. Possibly, it could be a new factor contributing to the generally weaker maximum negative Bouguer gravity values for impact structures associated with sedimentary targets (Pilkington and Grieve 1992). Lastly, the effect of central uplift of underlying basement has to be taken into account, as it can partly cancel the broad negative anomaly in the structure center, as described for example in the 6 km diameter Jebel Waqf as Suwwan structure (Heinrichs et al. 2014).

Modeling the Tunnunik impact structure and post-impact erosion

A possible geological solution explaining the observed gravity and magnetic field anomalies over the center of the Tunnunik impact structure is shown in Fig. 6. This numerical model is constrained by (1) gravity and magnetic field data, (2) average values of the bulk density for the Earth's layers such as the crust and the mantle (not shown in Fig. 6), (3) measured physical parameters for the different geological formations identified and sampled in the field, *i.e.*, bulk densities, magnetic susceptibility, natural remanent magnetization (NRM) intensity, inclination (I) and declination (D), and (4) field geological data and mapping, *i.e.*, thickness of geological formations (Dewing et al. 2013) and location of structures such as contacts and faults (Newman and Osinski 2016). Table 1 shows the measured physical parameters used in the model. Consistent with geological mapping, the model shows the remains of a central uplift with the Shaler Supergroup in the very centre. Clear lateral physical contrasts may reflect faults, particularly if they join some mapped faults on surface. Near the center (i.e., ±2 km from the profile center), the uplift of sedimentary units likely occurred along thrust faults (some are mapped and shown on Fig. 1). The crystalline basement core of this central uplift underlying the Shaler formation seems affected by brecciation and/or fracturing, as well as by an enhancement

of its magnetization intensity, required to explain the central magnetic anomaly detected on Fig. 4. The shape of the strongly-magnetized crystalline basement body contributes to the skewness of the anomaly (see profiles on Fig. 4B). Nearby this basement core, the deep part of the Shaler Supergroup unit also possesses a magnetization intensity larger than the overlying and surrounding parts, but about 10 times weaker than the one of the crystalline basement. More dolerite dykes may be present at depth in this unit. Overall, ~5 km from the center, coinciding with the shatter cone area, and from 0.7 to 1 km in depth at the center, the rocks seem more brecciated and fractured than outside, with 20 to 100 kg/m^3 density reduction (*i.e.* a maximum of 4% of porosity increase). This is probably the most striking result of this study: even if the Tunnunik impact structure is highly eroded and even if the Quaternary Sand Formation biases the general low gravity signal by producing isolated very low (down to -4.6 mGal) gravity values, a ~1 km-thick zone of brecciated and fractured uplifted rocks (including basement) seems to be present. The presence of crystalline basement rocks (denser than the overlying units despite brecciation) in the central uplift also accounts for the local gravity 'high' of –2.6 mGal at the center of the structure, within the general gravity low. There is also a transition zone of density reduction (~10 kg/m^3) between 5 and 10 km of lateral distance from the center, inside the rim of local faults that surrounds our studied area (see Figs. 1 and 2).

A second model was built along the W-E direction profiles and is shown in the Supplementary Material (Fig. S3). It reveals a structure similar to the one shown in the N-S model of Fig. 6, again with ~1 km-thick brecciated/fractured rocks at the center, and with an associated enhancement of magnetization. The combination of these 2 perpendicular profiles does support a small assymetry of the brecciated rocks towards N (Fig. 6), but not really towards W (Fig. S3). Of course, in the absence of data with higher spatial resolution (especially gravity data) and of borehole data, more detailed geological models (including 3D representation) are not possible. The pre-impact distribution of densities within the target rocks is also a key parameter in those models (Pilkington and Grieve 1992). Despite stratigraphic information from Dewing et al. (2013), our models show that sharp and significant (e.g. ~300 m for some layers in the central area) thickness variations are necessary to explain the observed anomalies. This variability is due to faulting which offsets formations, including the Mount Phayre Formation which has a weak density (~2,500 kg/m^3). The porous Quaternary sand units, possibly thicker than 100 m (as shown by EM34 measurement interpretation) and correlated with the very low gravity values, also play a role in decreasing the RMS residuals (of about 0.2 mGal) between observations and predictions of the Bouguer gravity signal.

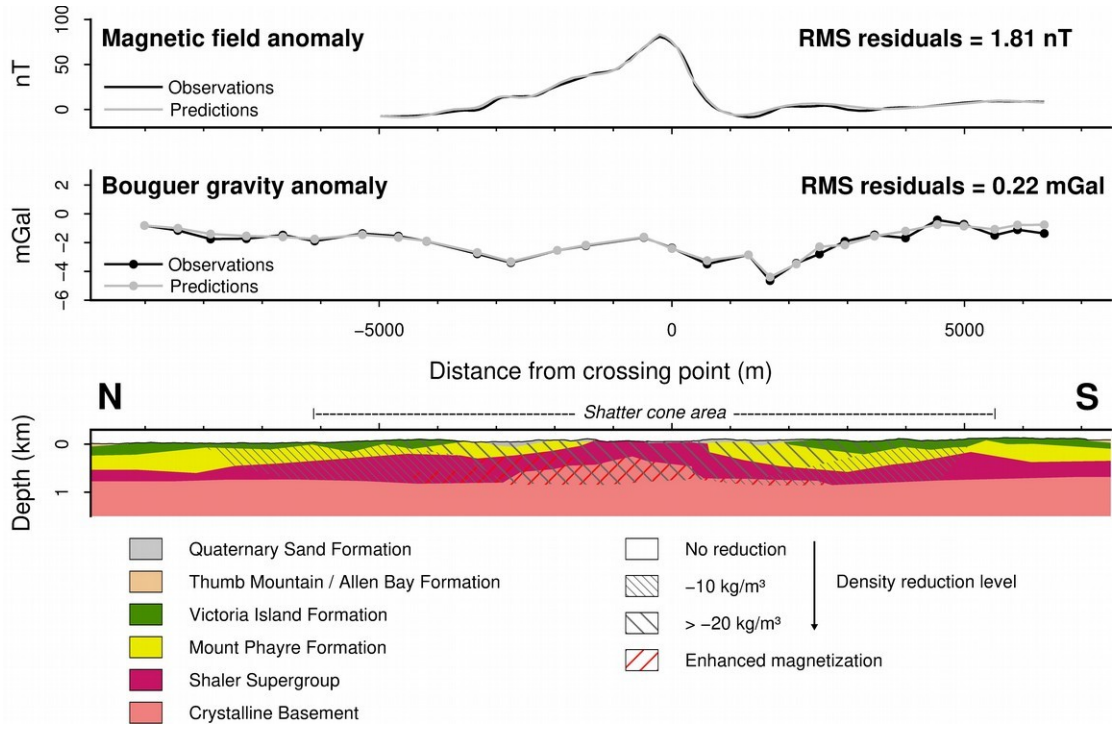


Fig. 6. N-S profile modeling of the Tunnunik impact structure constrained by magnetic and gravity data, as well as by laboratory measurements on samples. Top: comparison of observed (black) and predicted (gray) magnetic and gravity anomaly data. Location of the gravity measurements are shown by the solid points. Bottom: corresponding forward numerical model of the crust over the center of the Tunnunik impact structure. The physical parameters of each layer are shown in Table 1. Fracturing and brecciation (symbolized by gray hatching) decrease the bulk density values of all geological layers from the outer parts of the crater to the center. Topographic variations are from the global digital elevation model version 2 (GDEM2) of ASTER (NASA-METI). No vertical exaggeration.

Table 1. Physical parameters of the Tunnunik geological layers

Geological unit	D[1,2] (kg m^{-3})	K[1] (10^{-3} SI)	NRM[1] (A.m^{-1})	I[1] (°)	D[1] (°)
Quaternary sand formation	2000	-	-	-	-
Thumb Mountain / Allen Bay formation	2740-2760	0.02	< 10^{-3}	-	-
Victoria Island formation	2720-2750	0.01	< 10^{-3}	-	-
Mount Phayre formation	2470-2580	0.07	< 10^{-3}	-	-
Shaler Supergroup (with dolerite dykes)[3]	2630-2650	0.04 – 0.2	0.01 – 0.03	80-90	0
Crystalline basement[4]	2650-2700	50	0.1 – 0.5	90	0

[1]d, bulk density; K, volumic magnetic susceptibility; NRM, natural remanent magnetization; I and D, inclination and declination of NRM, respectively

[2]Minimum bulk density values are associated with rock samples collected nearby the center (i.e. distance < 5 km from modeling profile center), while maximum values correspond either to samples collected far from the center (i.e. d ~ 8-10 km) or to values expected from the forward modeling (e.g., for the upper crust basement).

[3]The Shaler Supergroup rocks are intruded by dolerite dykes of K = 4 10^{-2} SI, NRM = 0.7 A.m^{-1}, I~30°, D~110° (Lepaulard et al., 2019). Therefore we adjusted the parameters of the corresponding modeled layer by considering about 5% of dolerite dykes.

[4]The basement with an enhanced magnetization is correlated to the basement affected by brecciation (see Fig. 6).

Despite the simplicity of the models, there is a good agreement with computed estimations of brecciation/fracture depth extent in the presence of a low gravity anomaly. Indeed, according to the infinite slab model formula (see Supp. Mat. for calculation) for structures of $D_a \geq$ 20-30 km (Pilkington and Grieve 1992), a maximum density contrast of 100 kg m^{-3} (Table 1), associated with a maximum negative gravity value $\Delta g = -3$ to -4 mGal, gives a maximum depth extent Z = 715 to 954 m, a value in the range of the depth extent (0.7-1 km) of the brecciated/fractured zone of our models (Figs. 6 and S3). A density contrast of about 150 kg m^{-3} has been determined at Gosses Bluff (Barlow 1979), a structure similar to Tunnunik (see discussion above). However, the determination of density contrasts between unfractured and fractured target rocks remains sparse (see Pilkington and Grieve 1992 for a list). Similarly, for deeply eroded structures (E = 6-7; Grieve and Robertson 1979), the amount of removal of the disturbed zone beneath the crater floor is poorly constrained, allowing for significant variations in the corresponding gravity effect (Pilkington and Grieve 1992).

At Haughton, the expected post-impact erosion (~150 m; Osinski et al. 2005) together with the age of the structure (~ 23.5 Ma; Young et al. 2013) lead to an average erosion rate of 6.4 m Ma^{-1} since the time of the impact. Because Tunnunik is at high latitudes in an expected relatively stable tectonic environment of the Canadian Arctic since about 150-200 Ma, we can suppose as first approximation the same erosion rate as Haughton to obtain a minimum estimate of the erosion at Tunnunik. Using the paleomagnetic age of ~430 Ma for the Tunnunik impact structure (Lepaulard et al. 2019) with Haughton's erosion rate of 6.4 m Ma^{-1}, it gives ~2.7 km of post-impact erosion. Using only 200 Ma with the same rate, it leads to ~1.3 km. One could argue that this post-impact erosion is responsible for the weakness of the observed negative Bouguer gravity anomaly. However, because the impact indeed happened ~430 Ma in the Silurian or in the late Ordovician, the target was "only" composed of the Allen Bay (Ordovician-Silurian), Victoria Island (Ordovician), Stripy Unit (Cambrian) and Wynniat (Proterozoic) formations which are observed in the structure (Dewing et al. 2013). Therefore, only the younger impacted unit (Allen Bay) could have been partially eroded away. Its thickness is supposed to be of maximum ~1 km (Dewing et al. 2013). Combined with the possible uncertainty in paleomagnetic dating, this could give a maximum thickness of about 1 km for the target rocks possibly eroded away. One cannot assess the thickness of post-impact deposits, but between 430 and ~200 Ma, the Tunnunik impact structure moved from equatorial to high latitudes. It implies possible higher erosion rates during this period, which may compensate the deposition of sediments. The apparent crater diameter D_a shrinks with increasing depth of erosion Z_E by $D_a = D - 1.15\ Z_E$, because of the inclination of crater rim normal faults which dip toward the center of the crater by generally 60° (Kenkmann et al. 2013). According to this relation, and supposing Z_{Emin} = 1 km (erosion of target rocks), Z_{Emax} = 2.7 km (total erosion) and a D_a = 28 km, the final (rim-to-rim) diameter D of the fresh Tunnunik impact crater could have been between ~29 km and ~31 km.

Magnetization contrasts

The positive magnetic field anomaly detected over the center of the Tunnunik impact structure appears to almost exactly correlate to the outcrop area of the Wynniatt (part of the Shaler Supergroup) Formation (Figs. 1 and 4). Similar to Haughton, the most magnetic rock mapped

and collected in the area is dolerite (K = 4 10^{-2} SI and NRM = 0.7 A.m^{-1} in average). This mafic rock is present as localized dykes intrusive into the crystalline basement and into the Shaler Supergroup units (Dewing et al. 2013). To take into account these mafic dykes in our forward model, we considered that 5% of the volume of this formation was composed of dolerite, resulting in a maximum magnetization intensity of 0.03 A.m^{-1} with a magnetic susceptibility of 2 10^{-1} SI (Table 1). These values are several orders of magnitude higher than the NRM and K of all other sedimentary rocks present in the area (therefore considered with M = 0 A.m^{-1} in the modeling). However, our models show that an additional deeper strongly-magnetized (0.5 A.m^{-1}) source is needed to explain the shape and amplitude of the central magnetic anomaly (Figs. 6 and S3). As mentioned in the previous sections, we suggest that this could be uplifted crystalline basement rocks. Such magnetized crystalline blocks within the central uplift could be explained either by the intrusion of dykes of impact melt rocks and breccias with a significant thermal remanent magnetization (e.g., Shah et al. 2005), or by shock-induced magnetization of pre-impact rocks (Cisowski and Fuller 1978), or by an enhanced magnetization of the basement due to hydrothermal alteration (Quesnel et al. 2013). The latter has been shown to increase the NRM within impact melt rocks of the central uplift at the nearby Haughton impact structure (Zylberman et al. 2017). Another possibility would be a concentration of mafic, pre-impact magmatic rocks at local scale, possibly remagnetized by the impact. Of course, a combination of these different processes is still possible.

Conclusion

The first geophysical measurements within the Tunnunik impact structure indicate the existence of a central ~10 km wavelength negative Bouguer gravity anomaly of ~3 mGal and a positive magnetic anomaly of ~120 nT amplitude. It shows that, despite the highly-eroded state of the structure, the geophysical signature of the impact structure is still preserved. Using forward modeling constrained by petrophysics measurements, the geometry of the sources accounting for these anomalies is estimated. It reveals a fractured zone down to 0.7-1 km depth in its present-day state, and suggests that at least 1 km of erosion has occurred since 430-450 Ma, the time of impact. The positive magnetic field anomaly is suggested to be mainly due to uplifted crystalline basement, but also by the Shaler Supergroup sedimentary formation which is intruded by dolerite dykes. The origin of the magnetization's enhancement for the crystalline basement is still unknown, even if impact-generated hydrothermal activity is a good candidate.

To decipher the issues unveiled by these first measurements and by modeling, additional gravimetric data would be helpful and other geophysical methods could be used across the whole structure, like seismics and/or magnetotellurics which could reveal the deep velocity/conductivity contrasts between fractured/brecciated and pristine crystalline basement at depth.

Acknowledgments, Samples, and Data

IPEV is acknowledged for funding the field work (project "Tunnunik", #1139). Excellent logistical support from the Polar Continental Shelf Project is also gratefully acknowledged. This work has been carried out thanks to the support of the A*MIDEX grant (n°ANR-11-IDEX-0001-02) funded by the French Government "Investissements d'Avenir" program. MITACS and Campus France are thanked for facilitating international collaboration by providing the MITACS Globalink Research Award-Campus France to W.Z. The Scintrex CG-5 relative gravimeter was loaned by the Gravity-Mobile facility (GMOB) of RESIF-INSU

(CNRS). This work was also supported by the Programme National de Planétologie (PNP) of INSU-CNRS, co-funded by CNES, as well as by a CNRS Projet International de Coopération Scientifique (PICS n°263407 – GEOCRAT). Funding from the Natural Sciences and Engineering Research Council of Canada to GRO is gratefully acknowledged.

References

Acuna M. H., Connerney J. E. P., Wasilewski P., Lin R. P., Anderson K. A., Carlson C. W., McFadden J., Curtis D. W., Mitchell D., Reme H., Mazelle C., Sauvaud J. A., d'Uston C., Cros A., Medale J. L., Bauer S. J., Cloutier P., Mayhew M., Winterhalter D., and Ness N. F. 1998. Magnetic field and plasma observations at Mars: initial results of the Mars Global Surveyor Mission. *Science* 279: 1676-1680.

Barlow B. C. 1979. Gravity investigations of the Gosses Bluff impact structure, central Australia. *Journal of Australian Geology and Geophysics* 4: 323-339.

CAN-SCAN project 1965-1976. *Canadian-Scandinavian Digital Data*. Dept Energy, Mines and Resources of Canada. These data are stored at NOAA NCEI website (https://www.ngdc.noaa.gov/mgg/trk/aeromag/can-scan/can-scan.htm)

Choe B.-H., Tornabene L., Osinski G. R., and Newman J. 2019. Remote Predictive Mapping of the Tunnunik Impact Structure in the Canadian Arctic using Multispectral and Polarimetric SAR Data Fusion. *Canadian Journal of Remote Sensing*. doi:10.1080/07038992.2018.1544846

Cisowski S. M., and Fuller M. 1978. The effect of shock on the magnetism of terrestrial rocks. *Journal of Geophysical Research* 83: 3441-3458. doi:10.1029/JB083iB07p03441

Clark J. F. 1983. Magnetic survey data at meteoritic impact sites in North America. *Geomagnetic Service of Canada, Earth Physics Branch, Open File* 83-5*:* 1-32.

Croizet D., Renard F., and Gratier J.-P. 2013. Chapter 3 - Compaction and porosity reduction in carbonates: A review of observations, theory, and experiments. *Advances in Geophysics* 54: 181 238. doi:10.1016/B978-0-12-380940-7.00003-2

Dence M. R. 1972. *The nature and significance of terrestrial impact structures*. 24th Int. Geol. Congr., 77-89.

Dewing K., Pratt B. R., Hadlari T. Brent T., Bédard J., and Rainbird R. H. 2013. Newly identified "Tunnunik" impact structure, Prince Albert Peninsula, northwestern Victoria Island, Arctic Canada. *Meteoritics and Planetary Science* 48(2): 211-223. doi:10.1111/maps.12052

Featherstone W.E., and Dentith, M.C. 1997. A geodetic approach to gravity reduction for geophysics. *Computer Geosciences* 23: 1063-1070.

Gattacceca J., Lamali A., Rochette P., Boustie M., and Berthe L. 2007. The effects of explosive driven shocks on the natural remanent magnetization and the magnetic properties of rocks. *Physics of the Earth and Planetary Interiors* 162: 85-98. doi:10.1016/j.pepi.2007.03.006

Gattacceca J., Berthe L., Boustie M., Vadeboin F., Rochette P., and De Resseguier T. 2008. On

the efficiency of shock magnetization processes. *Physics of the Earth and Planetary Interiors* 166: 1-10. doi:10.1016/j.pepi.2007.09.005

Gattacceca J., Boustie M., Lima E., Weiss B. P., de Resseguier T., and Cuq-Lelandais J. P. 2010. Unraveling the simultaneous shock magnetization and demagnetization of rocks. *Physics of the Earth and Planetary Interiors* 182: 42-49. doi:10.1016/j.pepi.2010.06.009

Gattacceca J., Zylberman W., Coulter A.B., Demory F., Quesnel Y., Rochette P., Osinski G.R., and Brenuchon E. 2019. Paleomagnetism and rock magnetism of East and West Clearwater Lake impact structures. *Canadian Journal of Earth Sciences* 56(9); 983-993. doi:10.1139/cjes-2018-0291

GEOINT 2008. *Gravity station data format and anomaly computations.* National Geospatial-Intelligence Agency of the USA, 6.

Grieve R. A. F. 2006. *Impact structures in Canada.* 1st ed. St Johns: Geological Association of Canada.

Grieve R. A. F., and Pilkington M. 1996. The signature of terrestrial impacts. *AGSO Journal of Australian Geology and Geophysics* 16(4): 399-420.

Grieve R. A. F., and Robertson P. B. 1979. The Terrestrial Cratering Record. 1. Current Status of Observations. *Icarus* 38: 212-229. doi:10.1016/0019-1035(79)90179-9

Gudlaugsson S. T. 1993. Large impact crater in the Barents Sea. *Geology* 21(4): 291-294. doi:10.1130/0091-7613(1993)021<0291:LICITB>2.3.CO;2

Gulick S. P. S., Christeson G. L., Barton P. J., Grieve R. A. F., Morgan J. V., and Urrutia-Fucugauchi J. 2013. Geophysical characterization of the Chicxulub impact crater. *Reviews of Geophysics* 51: 31-52. doi:10.1002/rog.20007

Halls H. C. 1979. The Slate Islands meteorite impact site: A study of shock remanent magnetization. *Geophysical Journal International* 59(3): 553-591. doi:10.1111/j.1365-246X.1979.tb02573.x

Heinrichs T., Salameh E., and Khouri H. 2014. The Waqf as Suwwan crater, Eastern Desert of Jordan: aspects of the deep structure of an oblique impact from reflection seismic and gravity data. *International Journal of Earth Science* 103: 233-252. doi:10.1007/s00531-013-0930-4

Heiskanen W. A., and Moritz H. 1967. *Physical Geodesy.* Edited by J. Gilluly and A. O. Woodford. San Francisco: W. H. Freeman and Company.

Hemingway D. J., and Tikoo S. M. 2018. Lunar Swirl Morphology Constrains the Geometry, Magnetization, and Origins of Lunar Magnetic Anomalies. *Journal of Geophysical Research - Planets* 123. doi:10.1029/2018JE005604

Henkel H. 1992. Geophysical aspects of meteorite impact craters in eroded shield environment, with special emphasis on electric resistivity. *Tectonophysics* 216: 63-89. doi:10.1016/0040-1951(92)90156-Z

Henkel H., and Reimold, W.U. 2002. Magnetic model of the central uplift of the Vredefort impact structure, South Africa. *Journal of Applied Geophysics* 51: 43-62.

Henkel H., Reimold W. U., and Koeberl C. 2002. Magnetic and gravity model of the Morokweng impact structure. *Journal of Applied Geophysics* 49: 129-147. doi:10.1016/S0926-9851(01)00104-5

Hergarten S., and Kenkmann, T. 2015. The number of impact craters on Earth: Any room for further discoveries?. *Earth and Planetary Science Letters* 425: 187-192. doi:10.1016/j.epsl.2015.06.009

Hwang C., Wang C.-G., and Hsiao Y.-S. 2003. Terrain correction computation using Gaussian quadrature. *Computers and Geosciences* 29: 1259-1268.

Kenkmann T., Collins G. S., and Wünnemann K. 2013. The modification stage of crater formation. In *Impact cratering: processes and products*, edited by Osinski G.R. and Pierazzo E. Malaysia: Wiley-Blackwell. pp. 60-75

Kjær K. H. Larsen N. K., Binder T., Bjørk A. A., Eisen O., Fahnestock M. A., Funder S., Garde A. A., Haack H., Helm V., Houmark-Nielsen M., Kjeldsen K. K., Khan S. A., Machguth H., McDonald I., Morlighem M., Mouginot J., Paden J. D., Waight T. E., Weikusat C., Willerslev E., and MacGregor J. A. 2018. A large impact crater beneath Hiawatha Glacier in northwest Greenland. *Science Advances* 4: eaar8173. doi:10.1126/sciadv.aar8173

Langlais, B., Purucker, M. E., and Mandea, M., 2004. Crustal magnetic field of Mars. *Journal of Geophysical Research* 109. doi:10.1029/2003JE002048 (E02008).

Langlais B., and Thébault E. 2011. Predicted and observed magnetic signatures of martian (de)magnetized impact craters. *Icarus* 212: 568-578. doi:10.1016/j.icarus.2011.01.015

Lee P., and Osinski G. R. 2005. The Haughton-Mars Project: Overview of science investigations at the Haughton impact structure and surrounding terrains, and relevance to planetary studies. *Meteoritics and Planetary Science* 40: 1755-1758. doi:10.1111/j.1945-5100.2005.tb00144.x

Lepaulard, C., Gattacceca, J., Swanson-Hysell, N., Quesnel, Y., Demory, F. and Osinski, G. 2019. A Paleozoic age for the Tunnunik impact structure. *Meteoritics and Planetary Science* 54(4): 740-751. doi:10.1111/maps.13239

Marion C. L., Osinski G. R., and Linnen R. L. 2013. *Characterization of hydrothermal mineralization at the Prince Albert impact structure, Victoria Island, Canada (abstract #1635)*. 44th Lunar and Planetary Science Conference, The Woodlands, Texas.

McNeill J. D. 1980. *Electromagnetic terrain conductivity measurement at low induction numbers* (Technical Note TN-6). Mississauga, Ontario, Canada: Geonics Ltd.

Milton D. J., and Sutter J. F. 1987. Revised age for the Gosses Bluff impact structure, Northern Territory, Australia, based on $^{40}Ar/^{39}Ar$ dating. *Meteoritics* 22: 281-289.

Morgan J., and Rebolledo-Vieyra M. 2013. Geophysical studies of impact craters. In *Impact cratering: processes and products*, edited by Osinski G.R. and Pierazzo E. Malaysia: Wiley-Blackwell. pp. 211-222

Newman J. D., and Osinski G. R. 2016. *Geological mapping of the Tunnunik impact structure, Victoria Island, Canadian High Arctic (abstract #1591)*. 47th Lunar and Planetary Science Conference, The Woodlands, Texas.

Nicholas J. B., Purucker M. E., and Sabaka T. J. 2007. Age spot or youthful marking: Origin of Reiner Gamma. *Geophysical Research Letters* 34: L02205. doi:10.1029/2006GL027794

O'Neill C., and Heine C. 2005. Reconstructing the Wolfe Creek meteorite impact: Deep structure of the crater and effects on target rock. *Australian Journal of Earth Sciences* 52:699-709. doi:10.1080/08120090500170450

Osinski G. R., and Ferrière L. 2016. Shatter cones: (Mis)understood? *Science Advances 2*(8): 9 p. doi:10.1126/sciadv.1600616

Osinski G. R., and Grieve R. A. F. 2013. Comparison of mid-size terrestrial complex impact structures: a case study. In *Impact cratering: processes and products*, edited by Osinski G.R. and Pierazzo E. Malaysia: Wiley-Blackwell. pp. 290-305

Osinski G. R., and Pierazzo E. 2013. Impact cratering: processes and products. In *Impact cratering: processes and products*, edited by Osinski G.R. and Pierazzo E. Malaysia: Wiley-Blackwell. pp. 1-20

Osinski G. R., Lee P., Spray J. G., Parnell J., Lim D. S. S., Bunch T. E., Cockell C. S., and Glass B. 2005. Geological overview and cratering model for the Haughton impact structure, Devon Island, Canadian High Arctic. *Meteoritics and Planetary Science* 40: 1759-1776. doi:10.1111/j.1945-5100.2005.tb00145.x

Osinski G. R., Abou-Aly S., Francis R., Hansen J., Marion C. L., and Tornabene L. L. 2013. *The Prince-Albert structure, Northwest Territories, Canada: A new 28-km diameter complex impact structure (abstract #2099)*. 44th Lunar and Planetary Science Conference, The Woodlands, Texas.

Pesonen L. J., Marcos N., and Pipping F. 1992. Palaeomagnetism of the Lappajärvi impact structure, western Finland. *Tectonophysics* 216: 123-142. doi:10.1016/0040-1951(92)90160-8

Pilkington M., and Grieve R. A. F. 1992. The Geophysical Signature of Terrestrial Impact Craters. *Reviews of Geophysics* 30(2): 161-181. doi:10.1029/92RG00192

Pilkington M., and Hildebrand A. R. 2000. Three-dimensional magnetic imaging of the Chicxulub Crater. *Journal of Geophysical Research* 105(B10): 23,479-23,491. doi:10.1029/2000JB900222

Pohl J., Eckstaller A. and Robertson P. B. 1988. Gravity and magnetic investigations in the Haughton impact structure, Devon Island, Canada. *Meteoritics* 23: 235-238.

Pohl J., Poschlod K., Reimold W. U., Meyer C., and Jacob J. 2010. Ries crater, Germany: The Enkingen magnetic anomaly and associated drill core SUBO 18. *Special Paper of the Geological Society of America* 465: 141-163.

Quesnel Y., Gattacceca J., Osinski G. R., and Rochette P. 2013. Origin of the central magnetic anomaly at the Haughton impact structure, Canada. *Earth and Planetary Science Letters* 367: 116-122. doi:10.1016/j.epsl.2013.02.032

Raiskila S., Plado J., Ruotsalainen H., and Pesonen L. J. 2013. Geophysical Signatures of the Keurusselkä Meteorite Impact Structure - Implications for Crater Dimensions. *Geophysica* 49(1-2): 3-23.

Ravat D., Finn C., Hill P., Kucks R., Phillips J., Blakely R., Bouligand C., Sabaka T., Elshayat A., Aref A., and Elawadi E. 2009. A preliminary, full spectrum, magnetic anomaly grid of the United States with improved long wavelengths for studying continental dynamics--A website for distribution of data. *U.S. Geological Survey Open-File Report* 1258: 2 p.

Robertson P. B., and Roy J. L. 1979. Shock-diminished paleomagnetic remanence at the Charlevoix impact structure, Quebec. *Canadian Journal of Earth Science* 16(9): 1842-1856.

Schwiderski E. W. 1980, Ocean tides, II: A hydrodynamic interpolation model. *Marine Geodesy* 3: 219–255.

Shah A., Brozena J., Vogt P., Daniels D., and Plescia J. 2005. New surveys of the Chesapeake Bay impact structure suggest melt pockets and target-structure effect. *Geology* 33(5): 417-420. doi:10.1130/G21213.1

Sprunt E. S. 1977. Destruction of porosity through pressure solution. *Geophysics* 42(4): 726-741. doi:10.1190/1.1440742

Tamura Y. 1987. A harmonic development of the tide generating potential. *Bulletin d'Informations des Marées Terrestres* 99: 6813–6855.

Tikoo S.M., J. Gattacceca, Swanson-Hysell, N. L., Weiss, B. P., Suavet, C., and Cournède, C. 2015. Preservation and detectability of shock-induced magnetization. *Journal of Geophysical Research - Planets* 120. doi:10.1002/2015JE004840

Todd B.J., Pullan S.E., Hunter J.A. 1991. Electromagnetic studies across lakes and rivers in permafrost terrain, Mackenzie River Delta, Northwest Territories, Canada. *Expanded Abstracts of 61st Annual International Meeting, 10-14 Nov., Society of Exploration Geophysicists,* Tulsa, Oklahoma, US, 565-568. doi:10.1190/1.1889198

Ugalde H., Morris W. A., Pesonen L. J., and Danuor S. K. 2007. The Lake Bosumtwi meteorite impact structure, Ghana - Where is the magnetic source? *Meteoritics and Planetary Science* 42(4/5): 867-882.

Wenzel, H.-G. 1996. The Nanogal software: earth tide data processing package ETERNA 3.30. *Bulletin d'Informations des Marées Terrestres* 124: 9425–9439.

Young K. E., Soest M. C., Hodges K. V., Watson E. B., Adams B. A., and Lee P. 2013. Impact thermochronology and the age of Haughton impact structure, Canada. *Geophysical Research Letters* 40: 3836-3840. doi:10.1002/grl.50745

Zuber M. T., Smith D. E., Neumann G. A., Goossens S., Andrews-Hanna J. C., Head J. W., Kiefer W. S., Asmar S. W., Konopliv A. S., Lemoine F. G., Matsuyama I., Melosh H. J., McGovern P. J., Nimmo F., Phillips R. J., Solomon S. C., Taylor G. J., Watkins M. M., Wieczorek M. A., Williams J. G., Jansen J. C., Johnson B. C., Keane J. T., Mazarico E., Miljković K., Park R. S., Soderblom J. M., and Yuan D.-N. 2016. Gravity Field of the Orientale Basin from the Gravity Recovery and Interior Laboratory Mission. *Science* 354(6311): 438-441. doi:10.1126/science.aag0519

Zylberman W., Quesnel Y., Rochette P., Osinski G. R., Marion C., and Gattacceca J. 2017. Hydrothermally-enhanced magnetization at the center of the Haughton impact structure? *Meteoritics and Planetary Science 52*(10): 2147-2165. doi:10.1111/maps.12917

Figure captions

Fig. 1. Geological map of the Tunnunik impact structure, modified from Dewing et al. (2013) and Newman and Osinski (2016). Background corresponds to a Map Data ©2015 Google satellite image. Stratigraphy: Neoproterozoic → Shaler Supergroup (Neoproterozoic), Cambrian → Mount Phayre formation (Cambrian), Cambrian/Ordovician → Victoria Island formation (Cambrian/Ordovician), and Thumb Mountain/Allen Bay formation (Upper Ordovician/Silurian). The coordinate system for the geological map is UTM Zone 12 North projection with WGS84 datum, in meters. Upper left: Location of the structure on Victoria Island in the Canadian Arctic, with a geographic coordinate system on a WGS84 datum. Background corresponds to the ArcGIS online ESRI Ocean layer.

Fig. 2. Geophysical measurements performed at Tunnunik. Background corresponds to a digital elevation model version 2 (GDEM2) from ASTER (NASA-METI). Same coordinate system as for Fig. 1.

Fig. 3. (A) Complete Bouguer gravity anomaly map over the center of the Tunnunik impact structure. The thin pinkwhite lines corresponds to the gravity anomaly profiles selected for modeling and shown in (B). Faults are indicated by full black lines. The area where shatter cones were observed and collected is delimited by the dashed red line (Osinski and Ferrière 2016), while the limits of the Quaternary Sand Formation correspond to the thin green lines. Grayscaled background corresponds to the digital elevation model shown in Fig. 2. Same coordinate system as for Fig. 1. (B) Complete Bouguer gravity anomaly data along the selected profiles in (A).

Fig. 4. (A) Magnetic field anomaly map of the center of the Tunnunik impact structure. The green solid line corresponds to the locations of the data selected for modeling. Faults are indicated by full black lines. The area where of shatter cones were observed and collected is delimited by the dashed red line (Osinski and Ferrière 2016). The area where outcrops the Shaler Supergroup Formation is exposed is delimited by the dotted purple line. Grayscaled background corresponds to the digital elevation model shown in Fig. 2. Same coordinate system as for Fig. 1. (B) Magnetic field anomaly along the selected profiles in (A).

Fig. 5. (A) Map of the electrical conductivity variations at about 20 m in depth, in the central area of the impact structure. Bouguer gravity data are also shown to illustrate the correlation between some isolated low gravity values and the Quaternary Sand deposits. Dashed black line corresponds to the cross-section shown in (C). (B) Image of the conductive formation composed of Quaternary sediments nearby the central river. (C) W-E cross-section resulting from interpolation of conductivity data (vertical exaggeration ~ 2; points: data from different coil orientations at each location) acquired on the sand formation in the same area, along the dashed line in (A).

Fig. 6. N-S profile modeling of the Tunnunik impact structure constrained by magnetic and gravity data, as well as by laboratory measurements on samples. Top: comparison of observed (black) and predicted (gray) magnetic and gravity anomaly data. Location of the gravity measurements are shown by the solid points. Bottom: corresponding forward numerical model of the crust over the center of the Tunnunik impact structure. The physical parameters of each layer are shown in Table 1. Fracturing and brecciation (symbolized by gray hatching) decrease the bulk density values of all geological layers from the outer parts of the crater to the center. Topographic variations are from the global digital elevation model version 2 (GDEM2) of ASTER (NASA-METI). No vertical exaggeration.